Absolute Quantification in ^{1}H MRSI of the Prostate at 3T

Guillaume Lemaître
Paul Michael Walker
Heriot-Watt University, Universitat de Girona, Université de Bourgogne
g.lemaitre58@gmail.com

***Abstract*—Prostate cancer is the second most frequently diagnosed cancer amongst men in the world. Many techniques are existing and used in order to detect and stage prostate cancers. However, magnetic resonance imaging techniques propose a several non-invasive exams. Magnetic Resonance Spectroscopic Imaging (MRSI) allows to study the metabolite concentrations. ^{1}H-MRSI was performed on sixteen men with a suspected prostate cancer using a pelvic multi-channel phased-array (8 channels) coil. The aim of this study is to estimate absolute concentrations of choline and citrate using a method the most adapted to our acquisition data. Absolute quantification was done using water signal as reference. Different variations of choline and citrate concentrations were observed compare to the one from literature.**

I. Introduction

The World Health Organization (WHO) published in 2008 that prostate cancer was the second most frequently diagnosed cancer of men and the fifth most common cancer overall [1]. No less than 899,000 new cases where detected worldwide in 2008 [1]. Prostate cancer accounts for approximately 7.1% of all cancers diagnosed in 2008 and 3.4% of all cancers deaths in 2008 [1]. Risks factor for prostate cancer are multiple. The diagnosis of prostate cancers for men over 50 years old. Prostate cancer rate increases upto about 70 and declines thereafter [2]. It has also been shown that the probability to have a cancer is higher when a member of the family has been already diagnosed [2].

Main current methods helping to diagnose prostate cancers include digital rectal examination, prostatic specific antigen (PSA) test, biopsy and magnetic resonance imaging (MRI). A rectal examination may allow detection of harder nodules within the softer prostatic tissue. A higher-than-normal level of PSA can indicate an abnormality of the prostate. However, other factors than cancers can lead to an increasing level of PSA [3]. Hence both previous exams can lead to false positive and negative diagnoses. The only way to confirm a cancer is to carry out a biopsy. However, MRI technique which is a relative recent technique allow to be useful in detection and staging of prostate cancers [4].

The common method to characterize and detect tumor, relative quantification is done using ratio choline and citrate peak integration as shown on equation 1 and 2.

$$[ratio] = \frac{[Cho]}{[Cit]} \tag{1}$$

$$[ratio] = \frac{[Cho] + [Cre]}{[Cit]} \tag{2}$$

The use of ratios has the great advantage that the method is easy to implement. It is sensitive to metabolite concentration changes. However, ratios do not allow one to know precisely which variations of the metabolite concentrations occur. It has been shown that ratios were less sensitive to abnormalities [5].

In this study, we took the advantages of absolute quantification using MRI acquisition at 3 Telsa. We created a custumize method in order to analyze the data of prostate spectroscopy. Then, absolute concentrations will be computed using water signal as reference. Finally, we present new observations about the variations of choline and citrate concentration variations between healty and tumor tissue.

II. Materials and Patients

A. MRI Protocol

^{1}H MR spectroscopic imaging have been collected at the University Hospital of Dijon). The data were acquired on a clinical 3 Tesla whole body magnet (Siemens Magnetom Trio TIM, Erlangen, Germany) with a pelvic multi-channel phased-array (8 channels) coil.

The study was performed using a water and lipid suppressed double-spin-echo point-resolved spectroscopic (PRESS) sequence optimized for quantification detection of choline and citrate metabolites. Water and lipid were suppressed using a dual-band spectral spatial pulse technique. In order to eliminate signals from adjacent tissues, especially periprostatic lipids and the rectal wall up to eight outer voxel saturation pulses were used. Data sets were acquired as $16 \times 12 \times 16$ (interpolated to $16 \times 16 \times 16$) phase-encoded spectral arrays, an echo time (TE) of 140 milliseconds, an repetition time (TR) of 720 milliseconds and 13 minutes acquisition time. A spectral bandwidth of 1250 Hertz was used with 512 data points. A combination of an elliptic weighted averaged k-space acquisition scheme 3D filtering of the signal in k-space were used, the latter in order to reduce intervoxel signal combination. Shimming was carried out using the Siemenbens 3D Mapshim routine on a voxel adapted to the volume of the entire prostate gland. Additional unsuppressed water acquitions (at TE 30, 80 and 140 milliseconds) of 1.5 minutes was also performed in order to allow quantification with respect to prostate water.

Systematic verification of the global shim (ie. over the complete 3D PRESS-selected volume) revealed line widths at half-height of the water peak of the order of 20-30 Hertz, routinely. The line widths for individual voxels were of the order of 8-12 Hertz. The total examination time, including the time spent positioning the patient, was approximately 45 minutes.

B. Study Population

1) "Healthy" Patients: The data set was composed of eight patients who had negative biopsies. Mean subject age was 61.8 (range 53.3-71.1). PSA value ranged between 2.7 to 15.0 $ng.mL^{-1}$ (mean, 8.0 $ng.mL^{-1}$).

2) Patients with Cancers: The data set was composed of eight patients with biopsy proven cancer. Mean subject age was 70.9 (range 57.8-82.3). PSA value ranged between 0.4 to 74.0 $ng.mL^{-1}$ (mean, 15.8 $ng.mL^{-1}$). Gleason score estimated via the biopsies ranged from 6 to 7.

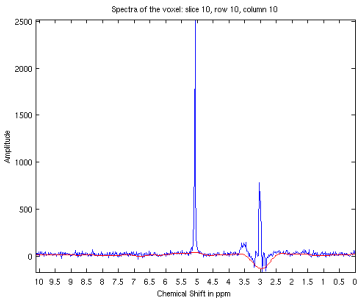

(a) Example of baseline detection using the method of Xi et al. [8].

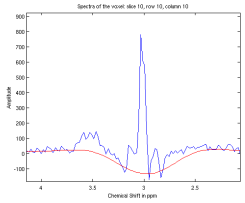

(b) The first criterion is that the baseline has to be smooth but not flat.

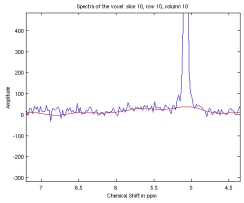

(c) The second criterion is that that the baseline has to run through the middle of the data in the portions where there is no signal.

Figure 1. Presentation of the method and criteria of Xi et al. method [8].

III. Analysis Method

Choline and citrate are considered as distinctive metabolites in the literature [6], [7]. It was pointed out that LCModel underestimate the citrate concentration during the quantification [4], [3]. That is why, our goal will be to implement an algorithm so as to obtain absolute concentration of these two metabolites. The following sections will present the scientific reasoning.

A. Baseline Detection

In order to obtain more accurate results for the integration of peaks, the baseline of the spectra has to be computed and substracted. Xi et al. propose to estimate the baseline and offer the advantage to customize the smoothness of the estimated baseline [8].

Xi et al. propose a statiscally based baseline detection derived from a parametric smoothing model [8]. They assumed a model where a measured spectra can be decomposed as the sum of a pure signal, the "baseline" or background and an additive Gaussian noise (equation 3).

$$y_i = b_i + \mu_i e^{n_i} + \varepsilon_i \tag{3}$$

where y_i is the signal, b_i is the baseline, μ_i is the true signal and n_i and ε_i are Gaussian noises.

Xi et al. built the cost function presented in equation 4 based on the assumption of the model chosen (equation 3) and that the baseline estimated should be smooth without being necessarily flat (figure 1(b)) and that should be laid on the middle of the data in segments where there is only noise (figure 1(c)) [8].

$$F(b) = \sum_i b_i - A\sum_i (b_{i+1}+b_{i-1}-2b_i)^2 - B\sum_i (b_i-\gamma_i)^2 g(b_i-\gamma_i) \tag{4}$$

where $g(\bullet)$ is the Heaviside function.

The cost function $F(b)$ is composed of three main terms:

- $\sum_i b_i$ is the sum of all baseline points.
- $-A\sum_i (b_{i+1} + b_{i-1} - 2b_i)^2$ is the smoothness penalty. This term tends to be small for linear segments while it will be large for small curvature radii.
- $-B\sum_i (b_i - \gamma_i)^2 g(b_i - \gamma_i)$ is the negative penalty. This term tends to be nonzero when the baseline is above the data point.

In order to compute the optimal baseline, the first term has to be maximized subject to both second and third terms (equation 5).

$$b_0 = \arg\max F(\mathbf{b}) \tag{5}$$

At this stage, the two parameter A and B have to be chosen. Xi et al. have shown that the theoritical values are as in equation 6 and 7.

$$A = \frac{5\times 10^{-9} n^4}{\sigma} \tag{6}$$

$$B = \frac{1.25}{\sigma} \tag{7}$$

where σ is an estimation of the standard deviation of the noise and n is the total number of data point.

Hence, an estimation of the standard deviation of the noise of the spectrum has to be performed. In order to estimate this parameter, Xi et al. proposed to divide the spectrum into smaller sections and compute the variance and mean intensity for each region. Then, they proposed to use the LOWESS regression to fit a model to the variance versus mean intensity signal. Finally, the estimation of the standard deviation of the noise is the square root of the variance at zero mean intensity in the LOWESS regression (equation 8).

$$\sigma = \sqrt{\sigma_\varepsilon^2} \tag{8}$$

where σ_ε^2 is the variance at zero mean intensity inferred using the LOWESS regression.

Once that all parameters are found, $\frac{\partial F(\mathbf{b})}{\partial \mathbf{b}} = 0$ has to be solved in order to maximize the function $F(\mathbf{b})$ [8].

B. Water Quantification

In order to calculate the absolute concentration using the tissue water as reference, a method allowing to integrate the water peak have to be implemented. In this part, we will explain only the method used to integrate the peak. The algorithm is described in algorithm 1.

The water has to be quantified on three sets of data where the echo time (TE) is the only variable. Indeed, the acquisitions were carried out at TE 30, 80 and 140 milliseconds. The longer is TE, the smaller will be the amplitude of the water peak as shown on figure 2. The position of the water peak is ca. 4.65 ppm. It might occur that the water peak could be shifted due to the non homogeneity of the magnetic field.

So as to integrate the water peak, the steps of the algorithm 1 have to be performed.

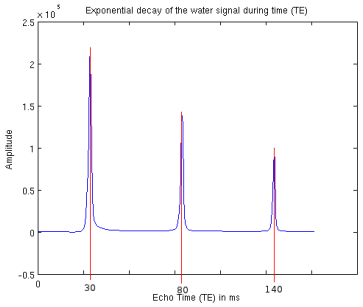

Figure 2. Example of the three different water peaks at different echo times (TE).Example of the three different water peaks at different echo times (TE). We can observed a decay exponential from echo time (TE) of 30, 80 and 140 milliseconds.

Algorithm 1 Water integral peak determination

for all spectra **do**
Crop the signal between range 3.96-5.94 ppm.
Compute a rough approximation of the signal using wavelet decomposition (Haar with 3 decomposition levels).
Detect valleys of the water peak using the algorithm of Lavielle [9].
Check if valleys are local minimum.
Detect the baseline using the algorithm of Xi and al. [8].
Substract the baseline to the original signal
Compute the numeric integral of the previous signal between the detected valleys.
end for

1) Approximation signal using Wavelet Decomposition and Synthesis: Firstly, the signal is cropped between 3.96 and 5.94 ppm since the water peak cannot occur outside of this range. Then, before detecting the valleys of the water peak, the signal is processed so as to obtain a rough signal where limits will be easier to distinguished. This rough signal is obtained by decomposing the original signal in the wavelet domain with the Haar family at the third level. Then, only approximation coefficients are used to reconstruct the signal. Comparison of these two signals are presented on figure 3(a).

2) Limits Detection: Lavielle proposed an algorithm to detect multiple changes inside data sequence [9]. This algorithm is used to find the limits in the previous signal computed which are the valleys of the water peak. However, it might occur that the detected limits are not real local minima. Thus, each limit is moved to the local minima analyzing previous and next sample iteratively. Figure 3(a) and 3(b) illustrate the valley detection.

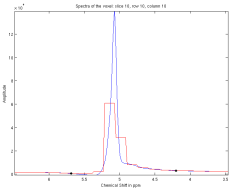

(a) Original signal is in blue. Red signal is the rough signal after wavelet analysis. Black crosses are the valleys detected using Lavielle's algorithm [9] follow by a research of local minimum.

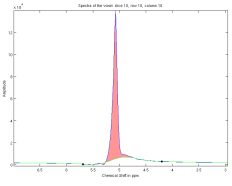

(b) Original signal is in blue. Green signal is the baseline detected using Xi et al. algorithm [8]. Red area will be integrated using Simpson's rule. Black crosses are the valleys detected after research of local minimum.

Figure 3. Water integration method

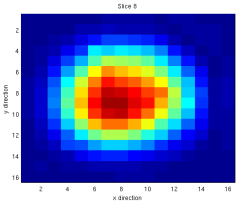

(a) Map of peak water integration.

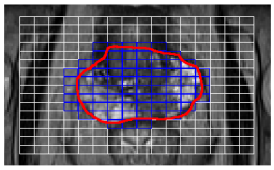

(b) Segmentation of prostate using K-means algorithm on peak water integration.

Figure 4. Water integration method

3) Numeric Integral Computation: The water peak will be integrated between the two limits previously detected. However, the baseline will be detected as presented in section III-A [8] and substracted from the original signal. The numeric integral will be computed using the Simpson's rule as shown on equation 9.

$$\int_b^a f(x)\,\mathrm{d}x = \frac{b-a}{6}\left[f(a) + 4f\left(\frac{a+b}{2}\right) + f(b)\right] \qquad (9)$$

Red area on figure 3(b) is the area which will be integrated.

C. Rough Prostate Segmentation

To reduce the time of computation and to exclude non-prostate voxels, a rough prostate segmentation was performed. We observed that the prostate was quite nicely delimited when observing the water intensity signal. The prostate position was estimated using a simple K-means algorithm. Example of segmantation is presented on figure 4.

D. Choline - Citrate Quantification

In this section, we will present our method allowing to extract the relative concentrations of choline and citrate.

Algorithm 2 Choline integral peak determination

for all spectra **do**
Crop the signal between range 3.17-3.29 ppm.
Detect maxima of the peak.
Detect valleys on each side of the maxima. These valleys are define to be the first nearest points of the baseline.
Crop the real choline peak.
Compute the baseline.
Substract the baseline to the signal cropped.
Fit a Gaussian $G(x)$ and Lorentzian $L(x)$ functions.
Compute the convolution $(G * L)(x)$ in order to obtain a Voigt profile $V(x)$.
Compute the numeric integral of $V(x)$ using Simpson's rule.
end for

1) Choline Quantification: Theoretically the peak of choline is localized at 3.21 ppm. Using this preknowledge, the signal was reduced to the range 3.17-3.29 ppm. The maxima of this range will be the apex of choline peak. The baseline is computed as described in section III-A [8] and substracted from the original signal. We will search iteratively each local minima on each side of the maximum. Then, only using the data between the limits detected, a Gaussian (equation 10) and a Lorentzian function (equation 11) will be fitted. In

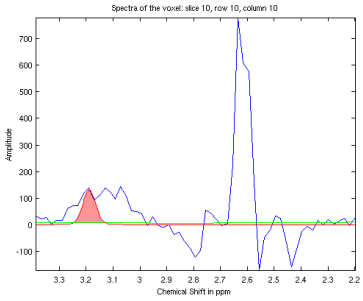

Figure 5. Fitting of Voigt function after detecting the choline peak.

order to find the different parameter for the Gaussian and Lorentzian function (equation 10 and 11), the algorithm of Levenberg-Marquardt was used.

$$G(x) = a\exp(-\frac{(x-b)^2}{2c^2}) \tag{10}$$

$$L(x) = \frac{1}{\pi}\frac{b}{(x-a)^2+b^2} \tag{11}$$

Peaks in NMR are considered to follow a Voigt function (equation 12) [10]. Thus, the convolution between the estimated Gaussian and Lorentzian function is performed.

$$V(x) = (G*L)(x) = \int_{-\infty}^{\infty} G(t)L(x-t)\,\mathrm{d}t \tag{12}$$

Having a discrete signal, the integration of the function $V(x)$ was computed using the Simpson's rule presented in equation 9. Figure 5 presents the fitting of a Voigt function to the choline peak.

Algorithm 3 Citrate integral peak determination

for all spectra **do**
  Smooth signal using cubic spline.
  Find minimum between 2.75-2.95 ppm and 2.40-2.50 ppm.
  Compute the baseline.
  From minimum find points the nearest to the baseline.
  Crop the real citrate peak.
  Substract the baseline to the cropped signal.
  Compute the numeric integral of the absolute previous signal using Simpson's rule.
end for

2) Citrate Quantification: The prior knowledge about the citrate peak is as follows:

- The citrate peak is a trident with small side lobes.
- The maximum of the citrate peak occurs at 2.64 ppm.
- The two minima of the two side lobes occur at 2.47 ppm and 2.81 ppm, respectively.

Using these hypothese, the original signal is cropped between 2.40 and 2.95 ppm. The signal is smoothed using a cubic spline function [11] (figure 6(a)). Using this smoothed function, the detection of minima is performed in the intervals 2.40-2.50 ppm and 2.75-2.95 ppm. The baseline of the absolute signal is computed (figure 6(a)). From the minima of the lower range (2.40-2.50 ppm), we will find the sample which will be the nearest to the baseline with a smaller abscissa. In the same way, from the minima of the higher range (2.75-2.95 ppm), we will find the sample wich will be the nearest to the

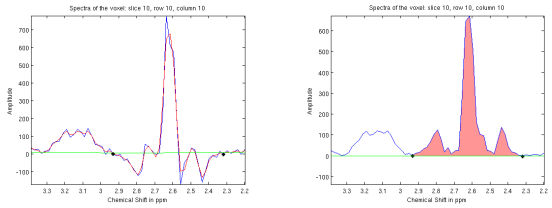

(a) The blue signal is the original signal. The red signal is the signal after a cubic spline smoothing. The green signal is the baseline of the absolute value of the original signal while the two black crosses are the limits detected.

(b) The blue signal is the signal obtained taking the absolute value of the substraction between the original signal and the baseline. The red area will be integrated using Simpson's rule between the two black crosses.

Figure 6. Citrate integration method

baseline with a larger abscissa. These two previous samples will be considered as limits of the citrate peak. The integration of the signal was computed using the Simpson's rule presented in equation 9. The integration will be computed on the absolute substraction between the original signal and the baseline previously computed between the two limits computed as shown on figure 6(b).

E. Absolute Quantification

In this section, normilzation by a tissue water reference will be presented. This normalization allows to obtain absolute quantification.

1) Absolute Quantification: Absolute quantification using water reference is based on the fact that the fully relaxed signal from water or metabolites is proportional to the number of moles of the molecules in the voxel [12]. Thus, we can deduce equation 13.

$$\begin{aligned}\frac{S_{0met}}{S_{0H_2O}} &= \frac{mol_{met}\times n_{Hmet}}{mol_{H_2O}\times 2}\\ [met] &= \frac{2\times[H_2O]\times S_{0met}}{n_{Hmet}\times S_{0H_2O}}\end{aligned} \tag{13}$$

where:

- S_0 is the fully relaxed signal.
- $[met]$ is the absolute concentration for each metabolite.
- H_2O is the tissue water concentration approximated at 39.4 $mol.kg^{-1}$ [13].
- n_{Hmet} is the number of protons associated with each metabolite, four protons for citrate and nine protons for choline.

Parameters which have to be computed are presented in the following sections.

2) Determinatation of S_{0H_2O}: The fully relaxed corrected signal of the water S_{0H_2O} can be obtained as expressed in equation 14.

$$S_{0H_2O} = \frac{S^*_{0H_2O}\exp(-\frac{TE}{T_2})}{1-\exp(-\frac{TR}{T_1})} \tag{14}$$

where:

- The numerator expresses T_2 correction (see next paragraph).
- TR is the repetition time set up for the examination which is 720 milliseconds.
- From previous studies, we observed that water T_1 was approximately 1600 milliseconds.

To obtain the numerator value of equation 14 corresponding to T_2 correction of the water signal, we computed the integral of the water

peaks as explained in section III-B for the three different TE 30, 80 and 140 milliseconds and fitted these data to an exponential decay of the form shown on equation 15.

$$y = a\exp(-bt) \tag{15}$$

The parameters a and b are obtained solving a non linear problem using the Levenberg-Marquardt's algorithm. In this case the parameter a corresponds to the numerator of equation 14.

3) Determinatation of S_{0met}: As in the previous section, the fully relaxed corrected signal of the metabolite considered S_{0met} can be obtained as expressed in equation 16.

$$S_{0met} = \frac{S^*_{0met}\exp(-\frac{TE}{T_2})}{1-\exp(-\frac{TR}{T_1})} \tag{16}$$

where:

- S^*_{0met} is obtained using methods of integration explained in section III-D regarding relative concentrations of choline and citrate.
- TE during the acquisition is set up at 140 milliseconds.
- T_2 is metabolite dependent. From the literature [14], citrate has a T_2 of 180 milliseconds and choline has a T_2 of 220 milliseconds.
- From previous studies, we observed that T_1 for choline was approximately 1500 milliseconds and for citrate was 600 milliseconds.

IV. Results

All results are presented using "box and whisker" plots. For each box, the central red mark is the median while the blue edges are the twenty-fifth and sevnty-fifth percentiles. The whiskers extend to the minima and maxima of the data.

A. Position (Apex-Median-Base) Behaviour

1) Peripheral Zone: Both citrate and choline concentrations seem to increase from the apex to the base of the prostate (25 % between apex-median and 15 % between median-base).

Furthermore, both citrate and choline concentrations tend to be higher (around 25 %) in healthy tissue of patients with negative biopsies than healthy tissue of patients with biopsy proven cancer.

Both choline and citrate concentrations are almost constant in the central gland in the three different zones apex, median and base. However, a very low increase (around 10 % respectively between apex-median and median-base) can be observed in healthy tissue of patients with negative biopsies through the different parts of the prostate. As in the peripheral zone, concentrations of patients with negative biopsies are higher than healthy tissue with biopsy proven cancer (around 20-30 %).

In order to find out the explenations of this phenomenon, an acquistion using a phantom with homogenous concentration of citrate and choline has to be performed and studied.

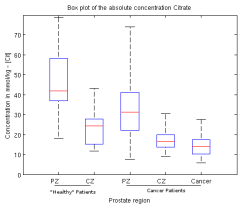

(a) Citrate variations through all the prostate. Comparison between negative biopsies and biopsy proven cancer patients.

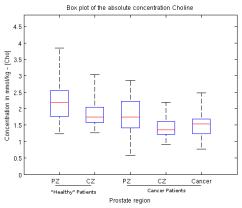

(b) Choline variations through all the prostate. Comparison between negative biopsies and biopsy proven cancer patients.

Figure 7. Comparison of absolute concentrations for choline and citrate between healthy and cancer tissue.

B. Peripheral Zone - Central Gland Behaviour

The mean value (± SD) of citrate concentration for peripheral zone was $45.34 \pm 14.83\ mmol.kg^{-1}$ which was significantly higher than that for central gland, at $24.00 \pm 8.76\ mmol.kg^{-1}$. The same observation can be done regarding the choline concentration where the mean value (± SD) for peripheral zone was $2.25 \pm 0.64\ mmol.kg^{-1}$ which was also significantly higher than that for central gland, at $1.87 \pm 0.42\ mmol.kg^{-1}$.

C. Cancer versus Healthy Tissue Behaviour

Kurhanewicz et al. [6], [7], Lowry et al. [13] and Liney et al. [15] present the discriminative role of citrate and choline. That is why, our study was focus in the different variations of these two metabolites. A comparison of our results and the results previouly given in the literature [6], [7], [13], [15] will be given. Results are presented in table I.

1) Citrate Concentration: Results obtained regarding citrate concentration in healthy and cancer tissues are in coordination with the work presented in the literature [13], [15]. Figure 7(a) are illustrated the different level of citrate concentration in the different prostate zone. The results are available inside the table I. The main observation which can be done is that the mean value (± SD) of citrate concentration in cancer tissue was $14.24 \pm 5.28\ mmol.kg^{-1}$ which was significantly lower than in peripheral zone, at $39.15 \pm 15.14\ mmol.kg^{-1}$ (figure 7(a)).

However, it is more difficult to distinguish the difference of concentrations between cancer tissue and tissue of the central gland. The mean value (± SD) in central zone was $20.71 \pm 7.04\ mmol.kg^{-1}$ while the concentration inside cancer tissue was $14.24 \pm 5.28\ mmol.kg^{-1}$(figure 7(a)).

An example for an healthy slice 8(b) and a cancer slice 8(d) is presented on figure 8. On these figures, the level of concentration is graduated where the blue color represent the minima concentration while red is the maxima. On figure 8(b), the peripheral zone can be characterized by a high level of citrate concentration compare to the central zone. On figure 8(d), the same distinction can be done. However, we can observed that the cancer zone present a relatively low level of citrate concentration and have a high contrast with the peripheral zone citrate concentration. Moreover, it is more difficult to distinguish the difference between cancer tissue and central gland tissue only observing citrate concentration.

Therefore, tumor tissue can be characteristic of a dicreasing concentration of citrate when occuring in the peripheral zone.

	Prostate Region			
Tissue Type	Apex	Median	Base	Overall
"Healthy" Patients				
Peripheral Zone	Choline: 1.70 ± 0.40 Citrate: 33.41 ± 10.10	Choline: 2.28 ± 0.56 Citrate: 45.67 ± 14.05	Choline: 2.60 ± 0.60 Citrate: 54.28 ± 12.94	Choline: 2.25 ± 0.64 Citrate: 45.34 ± 14.83
Central Gland	Choline:1.71 ± 0.34 Citrate: 21.34 ± 6.42	Choline: 1.87 ± 0.44 Citrate: 23.87 ± 9.38	Choline: 2.00 ± 0.45 Citrate: 26.42 ± 9.52	Choline: 1.87 ± 0.42 Citrate: 24.00 ± 8.76
Cancer Patients				
Peripheral Zone	Choline: 1.66 ± 0.32 Citrate: 23.67 ± 10.73	Choline: 1.80 ± 0.48 Citrate: 35.01 ± 11.52	Choline: 2.02 ± 0.82 Citrate: 39.20 ± 20.82	Choline: 1.82 ± 0.57 Citrate: 32.97 ± 15.45
Central Gland	Choline: 1.30 ± 0.29 Citrate: 19.70 ± 7.44	Choline: 1.45 ± 0.19 Citrate: 16.77 ± 3.82	Choline: 1.50 ± 0.41 Citrate: 16.16 ± 4.52	Choline: 1.42 ± 0.30 Citrate: 17.43 ± 5.31
Cancer Tissue	Choline: 1.57 ± 0.64 Citrate: 12.03 ± 8.39	Choline: 1.39 ± 0.37 Citrate: 13.24 ± 3.95	Choline: 1.54 ± 0.32 Citrate: 16.71 ± 4.90	Choline: 1.47 ± 0.40 Citrate: 14.24 ± 5.28

Table I
VARIATIONS OF CHOLINE AND CITRATE CONCENTRATIONS EXPRESSED IN $mmol.kg^{-1}$ DEPENDING OF THE REGION PROSTATE.

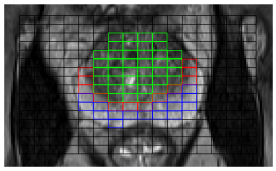

(a) Example of an anatomic view of an healthy patient. Blue voxels are peripheral zone, red voxels are merged zone while green zone is the central gland.

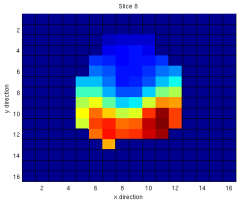

(b) Maps of the citrate concentrations. We can observed that the citrate concentration is higher than in the central gland.

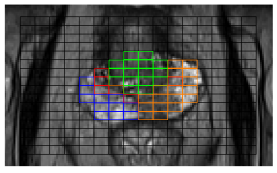

(c) Example of an anatomic view of a cancer prooved patient. Blue voxels are peripheral zone, red voxels are merged zone while green zone is the central gland.

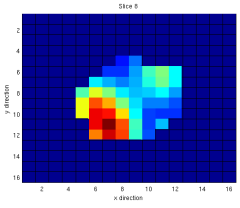

(d) Maps of the citrate concentrations. We can observed that the citrate concentration is higher than in the central gland. Furthermore, the cancer zone localized in the cancer zone is characterized by a low level of citrate concentration.

Figure 8. Citrate concentration variations at different part of the prostate between healthy and cancer proved cases.

D. Choline Concentration

Kurhanewicz et al. has been shown an increasing level of choline concentration between normal and cancer tissue [7]. Obtaining different results, we wanted to rise some points about the method used by Kurhanewicz et al. Indeed, in order to proof the variations of choline between healthy and cancer tissues, they compute ratios of choline concentration of different tissues (cancer, normal tissue, BPH, etc.) over the mean value of choline concentration of the normal peripheral zone of the same patient. Our results obtained in section IV-A tend to show a variability of choline and citrate concentrations according to the type of tissue or to the prostate position of the voxel. These variations could have an influence on the computation of the ratios.

In our results, we observed that the choline concentration is not varying in order to detect a cancer 7(b). Furthermore, we observed a small decreseasing level of choline concentration. The mean value ($\pm$ SD) of choline concentration in peripheral zone was $2.03 \pm 0.60\ mmol.kg^{-1}$ while the choline concentration in cancer tissue was $1.47 \pm 0.40\ mmol.kg^{-1}$. This change of choline concentration cannot be considered as distinctive.

V. CONCLUSION

A novel method to analyse the spectroscopy data of prostate has been done. A customize method using Voigt function fitting and integration allows to compute accurately absolute concentrations of choline and citrate metabolites since these two metabolites have been shown to be discriminative of prostate cancers [6], [7], [13], [15].

As shown in [13], [15], [7], we observed a significant decreasing level of citrate concentration from normal tissue to cancer tissue. However, this difference was only distinctive between the peripheral zone and the cancer zone. It was more difficult to observe a difference between the central gland and the cancer tissue.

The contribution of this work lie in the study of the variations of choline concentration. Indeed, Kurhanewicz et al. has been shown an increasing level of choline concentration in cancer tissue compare to normal tissue [7]. Our results shown that no significant increase was observed between cancer tissue and normal tissue. Furthermore, a small decreasing level of choline concentration was observed.

REFERENCES

[1] J. Ferlay, H. Shin, F. Bray, D. Forman, C. Mathers, and D. Parkin. (2010) Globocan 2008, cancer incidence and mortality worldwide: Iarc cancerbase no. 10 [internet]. International Agency for Research on Cancer. Lyon, France. [Online]. Available: http://globocan.iarc.fr

[2] AmericanCancerSociety, "Cancer facts and figures 2010," 2010. [Online]. Available: http://www.cancerquest.org/multimedia/pdf/facts&figures2010.pdf

[3] S. Parfait, J. Miteran, and P. Walker, "Classification de spectres et recherche de biomarqueurs en spectroscopie par résonance magnétique nucléaire du proton dans les tumeurs prostatiques," Ph.D. dissertation, Université de Bourgogne - LE2I, 2010.

[4] M. McLean, T. Barrett, V. Gnanapragasam, A. Priest, I. Joubert, D. Lomas, D. Neal, J. Griffiths, and E. Sala, "Prostate cancer metabolite quantification relative to water in 1 H-MRSI in vivo at 3 Tesla," *Magn Reson Med*, vol. 65, pp. 914–919, Apr 2011.

[5] J. F. Jansen, W. H. Backes, K. Nicolay, and M. E. Kooi, "1H MR spectroscopy of the brain: absolute quantification of metabolites," *Radiology*, vol. 240, pp. 318–332, Aug 2006.

[6] J. Kurhanewicz, D. B. Vigneron, S. J. Nelson, H. Hricak, J. M. MacDonald, B. Konety, and P. Narayan, "Citrate as an in vivo marker to discriminate prostate cancer from benign prostatic hyperplasia and normal prostate peripheral zone: detection via localized proton spectroscopy," *Urology*, vol. 45, pp. 459–466, Mar 1995.

[7] J. Kurhanewicz, D. B. Vigneron, H. Hricak, P. Narayan, P. Carroll, and S. J. Nelson, "Three-dimensional H-1 MR spectroscopic imaging of the in situ human prostate with high (0.24-0.7-cm3) spatial resolution," *Radiology*, vol. 198, pp. 795–805, Mar 1996.

[8] Y. Xi and D. M. Rocke, "Baseline correction for NMR spectroscopic metabolomics data analysis," *BMC Bioinformatics*, vol. 9, p. 324, 2008.

[9] M. Lavielle, "Detection of multiple changes in a sequence of dependent variables," *Stochastic Processes and their Applications*, vol. 83, no. 1, pp. 79–102, September 1999. [Online]. Available: http://ideas.repec.org/a/eee/spapps/v83y1999i1p79-102.html

[10] I. Marshall, J. Higinbotham, S. Bruce, and A. Freise, "Use of Voigt lineshape for quantification of in vivo 1H spectra," *Magn Reson Med*, vol. 37, pp. 651–657, May 1997.

[11] C. H. Reinsch, "Smoothing by spline functions," *Numerische Mathematik*, vol. 10, pp. 177–183, 1967.

[12] C. Gasparovic, T. Song, D. Devier, H. J. Bockholt, A. Caprihan, P. G. Mullins, S. Posse, R. E. Jung, and L. A. Morrison, "Use of tissue water as a concentration reference for proton spectroscopic imaging," *Magn Reson Med*, vol. 55, pp. 1219–1226, Jun 2006.

[13] M. Lowry, G. P. Liney, L. W. Turnbull, D. J. Manton, S. J. Blackband, and A. Horsman, "Quantification of citrate concentration in the prostate by proton magnetic resonance spectroscopy: zonal and age-related differences," *Magn Reson Med*, vol. 36, pp. 352–358, Sep 1996.

[14] T. W. Scheenen, G. Gambarota, E. Weiland, D. W. Klomp, J. J. Futterer, J. O. Barentsz, and A. Heerschap, "Optimal timing for in vivo 1H-MR spectroscopic imaging of the human prostate at 3T," *Magn Reson Med*, vol. 53, pp. 1268–1274, Jun 2005.

[15] G. Liney, L. W. Turnbull, M. Lowry, L. S. Turnbull, A. Knowles, and A. Horsman, "In vivo quantification of citrate concentration and water t2 relaxation time of the pathologic prostate gland using 1H MRS and MRI," *Magn Reson Imaging*, vol. 15, pp. 1177–1186, 1997.